J Inno Sci Eng, 2025, 9(2):171-186

DOI:https://doi.org/ 10.38088/jise.1581290

Research Article

Buckling and Free Vibration Analysis of Laminated Functionally Graded Carbon Nanotube-Reinforced Rectangular Plates

Ali Doğan[1*]

[1] *İskenderun Technical University, Department of Civil Engineering, 31200, İskenderun, Hatay, Türkiye*

ARTICLE INFO

Received Date: 7/11/2024
Accepted Date: 25/04/2025

Cite this paper as:
Doğan, A. (2025). Buckling and Free Vibration Analysis of Laminated Functionally Graded Carbon Nanotube-Reinforced Rectangular Plates. *Journal of Innovative Science and Engineering.* 9(2), 171-186.

*Corresponding author: Ali Doğan
E-mail:ali.dogan@iste.edu.tr

Keywords:
Buckling, Free vibration, FG-CNT material, Hamilton principle, Navier solution method, FEM.

ABSTRACT

This study investigated the buckling and free vibration of functionally graded carbon nanotube-reinforced composite (FG-CNTRC) rectangular plates under uniaxial loads. The current study researches the buckling and vibration behavior of CNTRC plates using single-walled CNTs (SWCNTs). SWCNTs were accepted to be regular and aligned, with a consistent pattern. CNT topologies were studied, including four different FG distributions of CNTs over thickness. Hamilton's principle was used to get the equations of motion for composite plates. The equations obtained for the solution were obtained by using the Navier solution method to solve the equation of motion. The results were compared using the FEM (Ansys) approach. The findings were proved to be compatible with FEM (Ansys). Then, it was understood from the parametric work that volume fractions, thickness ratios and FG distributions have a significant effect on the buckling and vibration response of FG-CNTRC plates. The findings were presented with graphs and tables.

1. Introduction

FG-CNTRC is an important material in the production of high-tech engineering components. It offers increased functionality and efficiency in a variety of applications. Recent advancements in nanotechnology enable the use of CNT materials in high-tech devices, making further research necessary to determine their engineering efficiency. Many scientists have conducted various studies to investigate the mechanical effects on FG-CNTRC reinforced plate-shell and beam in order to select the most suitable material for their applications. Yas et al. [1] investigated free vibrations and buckling in nanocomposite material Timoshenko beams reinforced with single-walled carbon nanotubes (SWCNTs) laying on an elastic basis. Lei et al. [2] examined the buckling behavior of thick skew plates

reinforced by functionally graded carbon nanotubes (FG-CNTs). Kumar and Srinivas [3] conducted a computational investigation of the dynamic and static response of beams built of FG-CNTR. Civalek et al. [4] presented the free vibration and buckling effects of CNTR cross-ply plates. Moradi-Dastjerdi and Malek-Mohammadi [5] used improved plate theory to examine free vibration and buckling behavior of FG-CNT plates using the refined shear deformation plate theory. Nguyen et al. [6] developed an analytical solution built on a 3D Finite Element model and Third Order Shear Dimensional theory. Foroutan et al. [7], nonlinear analysis of sandwich cylindrical panels whose core region consists of FG-CNTRC material was performed. Efraim and Eisenberger [8] presented exact vibration analysis of variable thickness thick annular isotropic and FGM plates. Nguyen, Karam and Bonnet [9] study on first-order shear deformation plate models for functionally graded materials. Zhang, Lei and Liew [10] researched buckling analysis of FG-CNT reinforced composite thick skew plates using an element-free approach. Kiani [11] presented free vibration of functionally graded carbon nanotube reinforced composite plates integrated with piezoelectric layers. Kiani [12] researched shear buckling of FG-CNT reinforced composite plates using Chebyshev-Ritz method. Kiani [13] presented buckling of FG-CNT-reinforced composite plates subjected to parabolic loading. Mota et al. [14] investigated porous functionally graded plates: an assessment of the influence of shear correction factor on static behavior. Sahan [15] suggested an alternative formulation for transient analysis of cross ply laminated shells. Sahan [16] investigated the dynamic analysis of linear viscoelastic cross-ply laminated shallow spherical shells. Dogan [17] researched free vibration and mode-shape analysis of plates and shallow shells. Dogan [18] investigated the mode-shapes behavior of double-curved shells. Dogan [19] analyzed the force vibration of laminated composite shells on elastic foundations. Dogan [20] presented the buckling analysis of symmetric laminated composite plates. Dogan [21] studied on buckling analysis of laminated plates. Dogan [22] investigated the responses of FGM plates for the viscoelastic case under the dynamic and quasi-static loads. Dogan and Sahan [23] investigated the viscoelastic damping response of FG-CNT shells. Dogan [24] researched dynamic response of laminated functionally graded carbon nanotube-reinforced composite viscoelastic plates. Dogan [25] presented dynamic and quasi-static behavior of laminated FG-CNTRC viscoelastic double-curved shells. An alternative solution method for the damped response of laminated Mindlin plates was presented by [26]. The dynamic analysis of viscoelastic functionally graded nanoplate was analysed by [27]. The inertio-elastic instability of functionally graded nanotube-reinforced composite disks was studied by [28]. A powerful numerical approach for the axisymmetric bending response of shear deformable two-directional functionally graded (2D-FG) plates with variable thickness was presented by [29]. Transient analysis of orthotropic, viscoelastic thick plates in the Laplace domain was investigated by [30]. Rasoli et al. [31] studied on static analysis of functionally graded porous beam-column frames by the complementary functions method. Xiao et al. [32] researched electric field-assisted alignment of carbon nanotubes in the interlayers of CFRP composites to enhance the properties. Cao et al. [33] investigated mechanical performance of diamine silane modified carbon Nanotubes reinforced epoxy resin composites.

In this study, the buckling and free vibration analysis of laminated FG-CNTRC plates was investigated. The FG-CNTRC material was put into the plate both layered and at an angle within each layer of CNT efficiency parameters (η) and volume fractions (Vcnt*) for various micromechanical models (Type 1-2-3) include were also added as parameters during the analyses. Buckling analysis of the FG-CNTRC plate, which combines all these features, has been carried out for the first time in the published works. The work progresses in the following stages: Firstly, the study's theoretical foundation was established. Secondly, critical buckling load values and free vibration values were found using Ansys and the approach used in this work for a variety of CNT FG distributions over the plate's thickness, and values found were compared to the results obtained using ANSYS. The approach employed in this study is totally congruent with the results obtained using the ANSYS. In the third step, a parametric study was performed to better comprehend the effect of thickness ratios and volume fractions on various micro-mechanical models and FG-CNT configurations.

2. FG-CNT Material Models

FGM is obtained by changing the composite material properties in line with the thickness of the plate. FG-CNT materials can be developed by adding carbon nanotubes to the element. Automotive, aerospace, biomedical nuclear, mechanical and civil engineering etc. FG-CNT materials are used in all areas. Figure 1 shows various material configurations of a rectangular FG-CNTRC plate. This study uses CNTs embedded in a polymer matrix. The CNTRC plate is made up of isotropic matrix and SWCNTs.

$$E_{11} = \eta_1 V_{cnt} E_{11}^{cnt} + V_m E^m \quad (1a)$$

$$\frac{\eta_2}{E_{22}} = \frac{V_{cnt}}{E_{22}^{cnt}} + \frac{V_m}{E^m} \quad (1b)$$

$$\frac{\eta_3}{G_{12}} = \frac{V_{cnt}}{G_{12}^{cnt}} + \frac{V_m}{G^m} \quad (1c)$$

Where, E_{11}^{cnt}, E_{22}^{cnt} and G_{12}^{cnt} represent the elasticity and shear modulus, respectively. Em and Gm symbolize the elasticity and shear modulus of the matrix material, respectively. Equation (3) includes the CNT efficiency parameters ηi (i=1,2,3). V_{cnt} is the volume fractions of a CNT. V_m is the volume fractions of matrix material. There is $V_m+V_{cnt} = 1$ formulation relationship between them. The mass density (ρ) and Poisson's ratio (ν) may be described as follows:

$$\nu = V_{cnt}\nu^{cnt} + V_m\nu^m \quad (2a)$$

$$\rho = V_{cnt}\rho^{cnt} + V_m\rho^m \quad (2b)$$

The Poisson's ratios are , ν^{cnt}, ν^m whereas the matrix and CNT densities are ρ^m ρ^{cnt} respectively. The distribution of CNTs in the plate's thickness direction illustrated in Figure 1 is presumed to be as follows:

$$FG-UD-: \quad V_{cnt} = V_{cnt}^* \quad (3a)$$

$$FG-O-: \quad V_{cnt} = 2\left(1-\frac{2|z|}{h}\right)V_{cnt}^* \quad (3b)$$

$$FG-X-: \quad V_{cnt} = 2\left(\frac{2|z|}{h}\right)V_{cnt}^* \quad (3c)$$

$$FG-\Delta-: \quad V_{cnt} = \left(1+\frac{2z}{h}\right)V_{cnt}^* \quad (3d)$$

The volume fraction of CNTs, denoted by V^*_{cnt}, is stated as follows:

$$V_{cnt}^* = \frac{W_{cnt}}{W_{cnt}+(\rho^{cnt}/\rho^m)(1-W_{cnt})} \quad (4)$$

W_{cnt} is the mass fraction of CNTs.

3. Theoretical Formulations

In plate theories, the mid-surface deflections of the plate can be written depending on the plate thickness. These thick plate theories may be higher order or not. In the current study, first order shear deformation theory (FSDT) was used. Equation 5 explains how FSDT works. FSDT takes into account both rotational inertia and transverse shear. The (ψx, ψy) and (u, v, w) symbolize the rotations and deflections of each point in the laminated plate, respectively. The deflections at the central surface of the plate are called wo, vo and uo, they are extremely minor compared to the thickness. Equation 5 allows the assumptions εz and σz equal zero to be applied. The vertical deflection in the z direction (w) is calculated using x, y and z directions. The shear angles and strains can be expressed at any location using median surface stresses, shear angles, and curvature changes (Equation 6).

$$u(x,y,z)=u_0(x,y)+z\,\psi_x\,(x,y) \quad (5a)$$

$$v(x,y,z)=v_0(x,y)+z\,\psi_y\,(x,y) \quad (5b)$$

$$w(x,y,z)=w_0(x,y) \quad (5c)$$

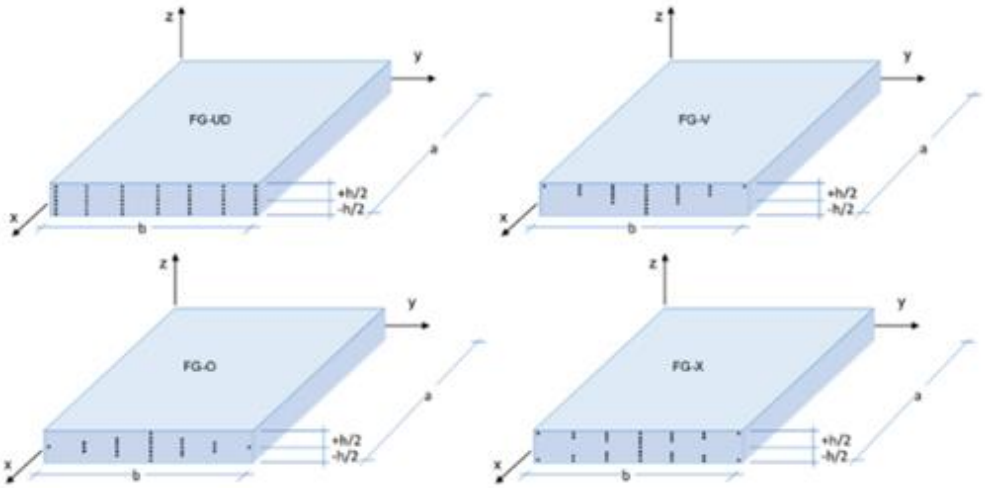

Figure 1. Illustration of FG-CNTRC configuration diversity for a plate.

$$\varepsilon_x = (\varepsilon_{0x} + z\kappa_x) \quad (6a)$$

$$\varepsilon_y = (\varepsilon_{0y} + z\kappa_y) \quad (6b)$$

$$\varepsilon_{xy} = (\varepsilon_{0xy} + z\kappa_{xy}) \quad (6c)$$

$$\varepsilon_{yx} = (\varepsilon_{0yx} + z\kappa_{yx}) \quad (6d)$$

$$\gamma_{xz} = \gamma_{0xz} \quad (6e)$$

$$\gamma_{yz} = \gamma_{0yz} \quad (6f)$$

Equation (7) depicts the curvatures and strains of the plate's center surface.

$$\varepsilon_{0x} = \frac{\partial u_0}{\partial x}, \varepsilon_{0y} = \frac{\partial v_0}{\partial y}, \varepsilon_{0xy} = \frac{\partial v_0}{\partial x}, \varepsilon_{0yx} = \frac{\partial u_0}{\partial y} \quad (7a)$$

$$\gamma_{0xz} = \frac{\partial w_0}{\partial x} + \psi_x, \ \gamma_{0yz} = \frac{\partial w_0}{\partial y} + \psi_y \quad (7b)$$

$$\kappa_x = \frac{\partial \psi_x}{\partial x}, \kappa_y = \frac{\partial \psi_y}{\partial y}, \kappa_{xy} = \frac{\partial \psi_y}{\partial x}, \kappa_{yx} = \frac{\partial \psi_x}{\partial y} \quad (7c)$$

With the help of the equation below, the σ-ε relationship of the plate can be calculated in x-y-z coordinates (Equation 8)

$$\begin{bmatrix} \sigma_x \\ \sigma_y \\ \tau_{yz} \\ \tau_{xz} \\ \tau_{xy} \end{bmatrix} = \begin{bmatrix} Q_{11} & Q_{12} & 0 & 0 & 0 \\ Q_{12} & Q_{22} & 0 & 0 & 0 \\ 0 & 0 & Q_{44} & 0 & 0 \\ 0 & 0 & 0 & Q_{55} & 0 \\ 0 & 0 & 0 & 0 & Q_{66} \end{bmatrix} \begin{bmatrix} \varepsilon_x \\ \varepsilon_y \\ \gamma_{yz} \\ \gamma_{xz} \\ \gamma_{xy} \end{bmatrix} \quad (8)$$

where, Q_{ij} are the lamina stiffness's,

$$Q_{11} = E_1(z)\frac{1-\vartheta_{23}(z)\vartheta_{32}(z)}{\Delta} \quad (9a)$$

$$Q_{12} = E_1(z)\frac{\vartheta_{21}(z)+\vartheta_{31}(z)\vartheta_{23}(z)}{\Delta} = E_2(z)\frac{\vartheta_{12}(z)+\vartheta_{32}(z)\vartheta_{13}(z)}{\Delta} \quad (9b)$$

$$Q_{22} = E_2(z)\frac{1-\vartheta_{31}(z)\vartheta_{13}(z)}{\Delta} \quad (9c)$$

$$Q_{13} = E_1(z)\frac{\vartheta_{31}(z)+\vartheta_{21}(z)\vartheta_{32}(z)}{\Delta} = E_3(z)\frac{\vartheta_{13}(z)+\vartheta_{12}(z)\vartheta_{23}(z)}{\Delta} \quad (9d)$$

$$Q_{23} = E_2(z)\frac{\vartheta_{32}(z)+\vartheta_{12}(z)\vartheta_{31}(z)}{\Delta} = E_3(z)\frac{\vartheta_{23}(z)+\vartheta_{21}(z)\vartheta_{13}(z)}{\Delta} \quad (9e)$$

$$Q_{33} = E_3(z)\frac{1-\vartheta_{12}(z)\vartheta_{21}(z)}{\Delta} \quad (9f)$$

$$Q_{44} = G_{23}(z) \quad (9g)$$

$$Q_{55} = G_{13}(z) \quad (9h)$$

$$Q_{66} = G_{12}(z) \quad (9i)$$

$$\Delta = 1 - \vartheta_{12}(z)\vartheta_{21}(z) - \vartheta_{23}(z)\vartheta_{32}(z) - \vartheta_{31}(z)\vartheta_{13}(z) - 2\vartheta_{21}(z)\vartheta_{32}(z)\vartheta_{13}(z) \quad (9j)$$

where E_1, E_2 and E_3 are young modulus in the 1,2,3 coordinates, G_{12}, G_{23} and G_{13} correspond to shear modulus and υ_{12}, υ_{21}, υ_{13}, υ_{31}, υ_{23}, υ_{32} represent to Poisson's ratios.

Figure 2 shows the angle (θ) between coordinate systems. Axis of 1 is fiber direction. The matrix of transformations can change the axe system from 1,2 to x, y directions (Equation 10).

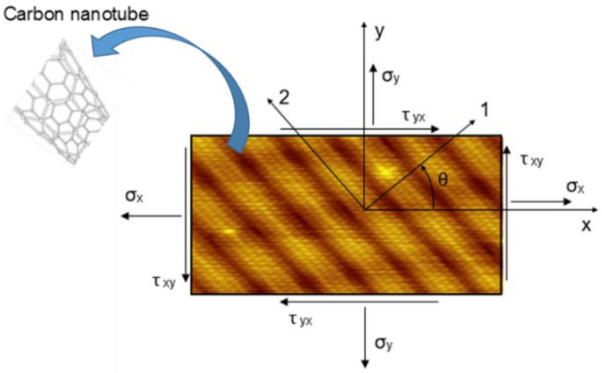

Figure 2. Illustration of axes of CNTR material in a layer (Dogan 2023)

$$T = \begin{bmatrix} c^2 & s^2 & 0 & 0 & 0 & 2cs \\ s^2 & c^2 & 0 & 0 & 0 & -2cs \\ 0 & 0 & 1 & 0 & 0 & 0 \\ 0 & 0 & 0 & c & -s & 0 \\ 0 & 0 & 0 & s & c & 0 \\ -cs & cs & 0 & 0 & 0 & (c^2 - s^2) \end{bmatrix} \quad (10)$$

The σ-ε connection for the nth layer may be determined using the Equation (11). In Equation (11), the terms $\bar{Q}_{ij}$ modified stiffness coefficients.

$$\begin{bmatrix} \sigma_x \\ \sigma_y \\ \sigma_z \\ \tau_{yz} \\ \tau_{xz} \\ \tau_{xy} \end{bmatrix} = \begin{bmatrix} \bar{Q}_{11} & \bar{Q}_{12} & \bar{Q}_{13} & 0 & 0 & \bar{Q}_{16} \\ \bar{Q}_{12} & \bar{Q}_{22} & \bar{Q}_{23} & 0 & 0 & \bar{Q}_{26} \\ \bar{Q}_{13} & \bar{Q}_{23} & \bar{Q}_{33} & 0 & 0 & \bar{Q}_{36} \\ 0 & 0 & 0 & \bar{Q}_{44} & \bar{Q}_{45} & 0 \\ 0 & 0 & 0 & \bar{Q}_{45} & \bar{Q}_{55} & 0 \\ \bar{Q}_{16} & \bar{Q}_{26} & \bar{Q}_{36} & 0 & 0 & \bar{Q}_{66} \end{bmatrix} \begin{bmatrix} \varepsilon_x \\ \varepsilon_y \\ \varepsilon_z \\ \gamma_{yz} \\ \gamma_{xz} \\ \gamma_{xy} \end{bmatrix} \quad (11)$$

Where,

$$\bar{Q}_{11} = Q_{11}c^4 + Q_{22}s^4 + 2(Q_{12} + 2Q_{66})s^2c^2 \quad (12a)$$

$$\bar{Q}_{12} = (Q_{11} + Q_{22} - 4Q_{66})s^2c^2 + Q_{12}(s^4 + c^4) \quad (12b)$$

$$\bar{Q}_{22} = Q_{11}s^4 + Q_{22}c^4 + 2(Q_{12} + 2Q_{66})s^2c^2 \quad (12c)$$

$$\overline{Q}_{13} = Q_{13}c^2 + Q_{23}s^2 \quad (12d)$$

$$\overline{Q}_{23} = Q_{23}c^2 + Q_{13}s^2 \quad (12e)$$

$$\overline{Q}_{33} = Q_{33} \quad (12f)$$

$$\overline{Q}_{16} = (Q_{11} - Q_{12} - 2Q_{66})c^3s - (Q_{22} - Q_{12} - 2Q_{66})s^3c \quad (12g)$$

$$\overline{Q}_{26} = (Q_{11} - Q_{12} - 2Q_{66})s^3c - (Q_{22} - Q_{12} - 2Q_{66})c^3s \quad (12h)$$

$$\overline{Q}_{36} = (Q_{13} - Q_{23})cs \quad (12i)$$

$$\overline{Q}_{66} = (Q_{11} + Q_{22} - 2Q_{12} - 2Q_{66})s^2c^2 + Q_{66}(s^4 + c^4) \quad (12j)$$

$$\overline{Q}_{44} = Q_{44}c^2 + Q_{55}s^2 \quad (12k)$$

$$\overline{Q}_{55} = Q_{55}c^2 + Q_{44}s^2 \quad (12l)$$

$$\overline{Q}_{45} = (Q_{55} - Q_{44})cs \quad (12m)$$

The moment and force results may be calculated by integrating the stresses over the plate thickness.

$$\begin{bmatrix} N_x \\ N_{xy} \\ Q_x \end{bmatrix} = \int_{-h/2}^{h/2} \begin{bmatrix} \sigma_x \\ \sigma_{xy} \\ \sigma_{xz} \end{bmatrix} dz \quad (13a)$$

$$\begin{bmatrix} N_y \\ N_{yx} \\ Q_y \end{bmatrix} = \int_{-h/2}^{h/2} \begin{bmatrix} \sigma_y \\ \sigma_{xy} \\ \sigma_{yz} \end{bmatrix} dz \quad (13b)$$

$$\begin{bmatrix} M_x \\ M_{xy} \\ P_x \end{bmatrix} = \int_{-h/2}^{h/2} \begin{bmatrix} \sigma_x \\ \sigma_{xy} \\ \sigma_{xz} \end{bmatrix} zdz \quad (14a)$$

$$\begin{bmatrix} M_y \\ M_{yx} \\ P_y \end{bmatrix} = \int_{-h/2}^{h/2} \begin{bmatrix} \sigma_y \\ \sigma_{xy} \\ \sigma_{yz} \end{bmatrix} zdz \quad (14b)$$

In equation (13, 14), Q_x and Q_y are transverse shear forces. P_x, and P_y are higher-order shear expressions. M_x, M_y and M_{xy} are moments and N_x, N_y, N_{xy} are normal forces. Potential energy Equation (15) and Lagrangian function Equation (16) can be expressed by the following equation:

$$\Pi = U - W \quad (15)$$

$$L = T - \Pi \quad (16)$$

By setting the integral of the Lagrangian function equal to zero, Hamilton's principle can be applied to the equation for the solution.

$$\delta \int_{t_1}^{t_2} (T + W - U)\, dt = 0 \quad (17)$$

In equation (17), T represents kinetic energy expression (Equation 18) and W defines the work done by external forces (Equation 19) can be expressed by the following equation;

$$T = \frac{\rho}{2} \int_V \left\{\frac{\partial u}{\partial t}\right\}^2 + \left\{\frac{\partial v}{\partial t}\right\}^2 + \left\{\frac{\partial w}{\partial t}\right\}^2 dxdydz \quad (18)$$

$$W = \int_x \int_y \left(q_x u_0 + q_y v_0 + q_z w_0 + m_x \psi_x + m_y \psi_y\right) ABdxdy \quad (19)$$

The moments are m_x, m_y, and the external forces are q_x, q_y, q_z. In Equation (20), U represents strain energy.

$$U = \frac{1}{2} \int_V \{\sigma_x \varepsilon_x + \sigma_y \varepsilon_y + \sigma_z \varepsilon_z + \sigma_{xy}\gamma_{xy} + \sigma_{xz}\gamma_{xz} + \sigma_{yz}\gamma_{yz}\} dV \quad (20)$$

Equation (21), also defined as the plate's governing formulations, can be obtained by solving Equation (17). An explicit version of Equation (17) can be written as follows;

$$\frac{\partial}{\partial x}(N_x) + \frac{\partial}{\partial y}(N_{yx}) + q_x = I_1 \ddot{u}^2 + I_2 \ddot{\Psi}_x{}^2 \quad (21a)$$

$$\frac{\partial}{\partial x}(N_y) + \frac{\partial}{\partial x}(N_{xy}) + q_y = I_1 \ddot{v}^2 + I_2 \ddot{\Psi}_y{}^2 \quad (21b)$$

$$\frac{\partial}{\partial x}(Q_x) + \frac{\partial}{\partial y}(Q_y) + q_z = I_1 \ddot{w}^2 \quad (21c)$$

$$\frac{\partial}{\partial x}(M_x) + \frac{\partial}{\partial y}(M_{yx}) - Q_x + m_x = I_2 \ddot{u}^2 + I_3 \ddot{\Psi}_x{}^2 \quad (21d)$$

$$\frac{\partial}{\partial y}(M_y) + \frac{\partial}{\partial x}(M_{xy}) - Q_y + m_y = I_2 \ddot{v}^2 + I_3 \ddot{\Psi}_y{}^2 \quad (21e)$$

The terms in equation (21) can be explained in equation (22 and 23) as follows:

$$\begin{bmatrix} N_x \\ N_y \\ N_{xy} \\ M_x \\ M_y \\ M_{xy} \end{bmatrix} = \begin{bmatrix} A_{11} & A_{12} & A_{16} & B_{11} & B_{12} & B_{16} \\ A_{12} & A_{22} & A_{26} & B_{12} & B_{22} & B_{26} \\ A_{16} & A_{26} & A_{66} & B_{16} & B_{26} & B_{66} \\ B_{11} & B_{12} & B_{16} & D_{11} & D_{12} & D_{16} \\ B_{12} & B_{22} & B_{26} & D_{12} & D_{22} & D_{26} \\ B_{16} & B_{26} & B_{66} & D_{16} & D_{26} & D_{66} \end{bmatrix} \begin{bmatrix} \varepsilon_{0x} \\ \varepsilon_{0y} \\ \gamma_{0xy} \\ \kappa_x \\ \kappa_y \\ \kappa_{xy} + \kappa_{yx} \end{bmatrix} \quad (22)$$

$$\begin{bmatrix} Q_x \\ Q_y \end{bmatrix} = \begin{bmatrix} A_{55} & A_{45} \\ A_{45} & A_{44} \end{bmatrix} \begin{bmatrix} \gamma_{0xz} \\ \gamma_{0yz} \end{bmatrix} \quad (23)$$

$$A_{ij} = \int_{h/2}^{-h/2} Q_{ij}(z)\, dz \quad (24a)$$

$$B_{ij} = \int_{h/2}^{-h/2} Q_{ij}(z)\, zdz \quad (24b)$$

$$D_{ij}=\int_{h/2}^{-h/2} Q_{ij}(z)\, z^2 dz \quad (24c)$$

$$A_{ij}=\int_{h/2}^{-h/2} K_i K_j Q_{ij}(z)\, dz \qquad i,j=4,5 \quad (24d)$$

In equation (24), K are the shear correction factors (K_i and K_j). K values were used as 5/6 in this study, as suggested by Timoshenko (1921). The inertia of the mass moment is also I in equation (25) as follow;

$$[I_1, I_2, I_3]=\int_{h/2}^{-h/2} \rho(z)\,[1, z, z^2]dz \quad (25)$$

ρ(z) is the density. Solutions can be obtained with the help of the Navier method, which is a solution made using trigonometric functions. The thick plate is designed as simply supported, the boundary conditions of the plate can be written as in Equation (26).

$$N_x = w_0 = v_0 = M_x = \psi_y = 0 \quad at\ x=0, \quad (26a)$$

$$N_y = w_0 = u_0 = M_y = \psi_x = 0 \quad at\ y=0, b \quad (26b)$$

Equation (26) and Figure 3 shows the boundary conditions for the case of simply supported.

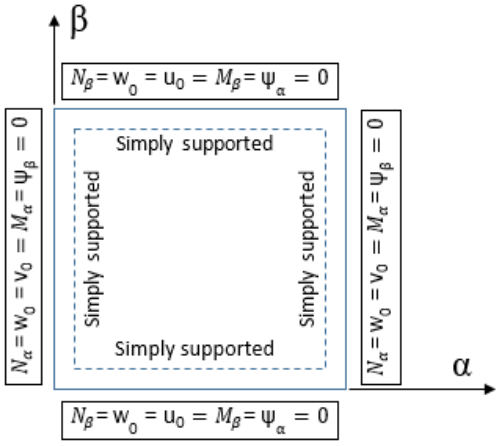

Figure 3. Illustration of boundary conditions of plate

To find the displacement and stress components, the displacement functions defined as Fourier series can be used in equation (27) as below:

$$u_0(x,y)=\sum_{m=0}^{\infty}\sum_{n=0}^{\infty} U_{mn}\cos(x_m x)\sin(y_n y) \quad (27a)$$

$$v_0(x,y)=\sum_{m=0}^{\infty}\sum_{n=0}^{\infty} V_{mn}\sin(x_m x)\cos(y_n y) \quad (27b)$$

$$w_0(x,y)=\sum_{m=0}^{\infty}\sum_{n=0}^{\infty} W_{mn}\sin(x_m x)\sin(y_n y) \quad (27c)$$

$$\psi_x(x,y)=\sum_{m=0}^{\infty}\sum_{n=0}^{\infty} W_{mn}\cos(x_m x)\sin(y_n y) \quad (27d)$$

$$\psi_y(x,y)=\sum_{m=0}^{\infty}\sum_{n=0}^{\infty} W_{mn}\sin(x_m x)\cos(y_n y) \quad (27e)$$

In equation (27), y_n = n/b and x_m = m/a. Substituting equations (22) – (27) into equations of motion (21), and eigenvalue equations are found for free vibration case by equation (28);

$$[K_{mn}]-\omega_{mn}^2[M_{mn}]\{\Delta_{mn}\}=\{0\} \quad (28)$$

and for buckling problem, the equations of motion are written in Equation (29) as below;

$$[K_{mn}]-\omega_{mn}[N_{mn}]\{\Delta_{mn}\}=\{0\} \quad (29)$$

Where,

$$M=\begin{bmatrix} M_{11} & 0 & 0 & M_{14} & 0 \\ 0 & M_{22} & 0 & 0 & M_{25} \\ 0 & 0 & M_{33} & 0 & 0 \\ M_{41} & 0 & 0 & M_{44} & 0 \\ 0 & M_{52} & 0 & 0 & M_{55} \end{bmatrix} \quad (30a)$$

$$[N]=\begin{bmatrix} 0 & 0 & 0 & 0 & 0 \\ 0 & 0 & 0 & 0 & 0 \\ 0 & 0 & \alpha^2\bar{N}_x+\beta^2\bar{N}_y & 0 & 0 \\ 0 & 0 & 0 & 0 & 0 \\ 0 & 0 & 0 & 0 & 0 \end{bmatrix} \quad (30b)$$

$$[K]\begin{bmatrix} K_{11} & K_{12} & K_{13} & K_{14} & K_{15} \\ K_{21} & K_{22} & K_{23} & K_{24} & K_{25} \\ K_{31} & K_{32} & K_{33} & K_{34} & K_{35} \\ K_{41} & K_{42} & K_{43} & K_{44} & K_{45} \\ K_{51} & K_{52} & K_{53} & K_{54} & K_{55} \end{bmatrix} \quad (30c)$$

$$[\Delta]=\begin{bmatrix} U_{mn} \\ V_{mn} \\ W_{mn} \\ \psi_{xmn} \\ \psi_{ymn} \end{bmatrix} \quad (30d)$$

In equations (30), $[M_{mn}]$, $[N_{mn}]$, $[K_{mn}]$, $[\Delta_{mn}]$ represent mass, buckling load, stiffness, displacement matrixes respectively. The stiffness matrix terms are given in equations (31) below;

$$K_{11}=-A_{11}x_m^2-A_{16}x_m y_n-A_{66}y_n^2 \quad (31a)$$

$$K_{12}=K_{21}=-A_{16}x_m^2-(A_{12}+A_{66})x_m y_n-A_{26}y_n^2 \quad (31b)$$

$$K_{13}=K_{31}=0 \quad (31c)$$

$$K_{14}=K_{41}=-B_{11}x_m^2-2B_{16}x_m y_n-B_{66}y_n^2 \quad (31d)$$

$$K_{15}=K_{51}=-B_{16}x_m^2-(B_{12}B_{66})\,x_m y_n-B_{26}y_n^2 \quad (31e)$$

$$K_{22}=-A_{66}x_m^2-A_{26}x_m y_n-A_{22}y_n^2 \quad (31f)$$

$$K_{23}=K_{32}=0 \quad (31g)$$

$$K_{24}=K_{42}=-(B_{12}+B_{66})\,x_m y_n \quad (31h)$$

$$K_{25}=K_{52}=-B_{66}x_m^2-B_{22}y_n^2 \quad (31i)$$

$$K_{33}=-A_{55}x_m^2-2A_{45}x_m y_n-A_{44}y_n^2 \quad (31j)$$

$$K_{34}=K_{43}=-A_{55}x_m-A_{45}y_n \quad (31k)$$

$$K_{35}=K_{53}=-A_{44}y_n-A_{45}x_m \quad (31l)$$

$$K_{44}=-A_{55}-D_{11}x_m^2-2D_{16}\,x_m y_n-D_{66}y_n^2 \quad (31m)$$

$$K_{45}=K_{54}=-A_{45}-D_{16}x_m^2-(D_{12}+D_{66})\,x_m y_n-D_{26}y_n^2 \quad (31n)$$

$$K_{55}=-A_{44}-D_{66}x_m^2-2D_{26}\,x_m y_n-D_{22}y_n^2 \quad (31o)$$

$$M_{11}=M_{22}=M_{33}=-I_1, M_{14}=M_{25}=-I_2, M_{44}=M_{55}=-I_3 \quad (31p)$$

$$M_{ij}=M_{ji}, \quad (31r)$$

4. Numerical Solutions and Discussions

The current study focused on uniaxial buckling analysis and vibration analysis of FG-CNT (Figure 4). The codes have been developed using a Mathematica [34] to solve the technique suggested in this paper. The findings were compared to ANSYS [35] finite element software. The buckling and free vibration analysis results for FG-CNT plates generated by the technique suggested in this paper were compared to those obtained using the FEM. FEM analysis was performed using the ANSYS 23 version software. In this study, SHELL281 Element Description is suitable for analyzing thin to moderately-thick shell structures (Figure 6). The element has eight nodes quadratic element with six degrees of freedom at each node: translations in the x, y, and z axes, and rotations about the x, y, and z-axes (ANSYS (2023)). The plate shapes have been divided into 40x40 mesh pieces (Figure 5). The effect of thickness and volume fractions on several FG-CNT combinations and micromechanical models were explored. The matrix material used in the investigation was poly methyl methacrylate (PMMA), and its material properties are E_m=2.5GPa, ν_m=0.3, ρ_m=1.190 kg/m^3. The material characteristics of SWCNTs are as follows: $E_{11}^{cnt}=600\,GPa$, $E_{22}^{cnt}=10\,GPa$, $G_{12}^{cnt}=17.2\,GPa$, $\rho_{cnt}=1.400\ kg/m^3$ and ν_{cnt}= 0.19. In the study, symmetric (0°/0°/0°/0°/0°) and (0°/90°/0°/90°/0°) cross-ply layered simply supported samples was used. This study employed three different types of micromechanical models (Table 1). In the study, Equation (32) was used to non-dimensional the buckling and free vibration results, respectively:

$$\lambda=\bar{N_x}\frac{b^2}{E_m h^3},\ \Omega=\omega b^2\sqrt{\rho_m/E_m h^2} \quad (32)$$

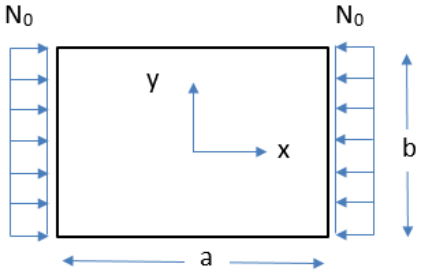

Figure 4. The loading conditions of plate

FG-CNT has a more complicated configuration than traditional FGM. In this work, Vf and η parameters, as well as several micromechanical models, were studied. Figure 7 displays the variation in the distribution of Vf (volume fractions) throughout thickness for FG-CNTRC configurations. Parametric analysis was done to clarify and emphasize the effect of Vf, and configurations of FG (FG-OD, FG-VD, FG-UD and FG-XD) on the free vibration and buckling behavior of the FG-CNT plate. By evaluating the data found, the following conclusions were reached.

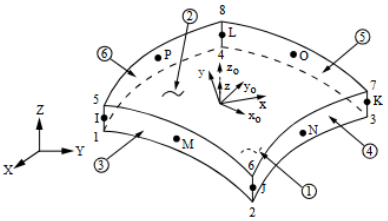

Figure 6. SHELL281 element description in ANSYS simulation.

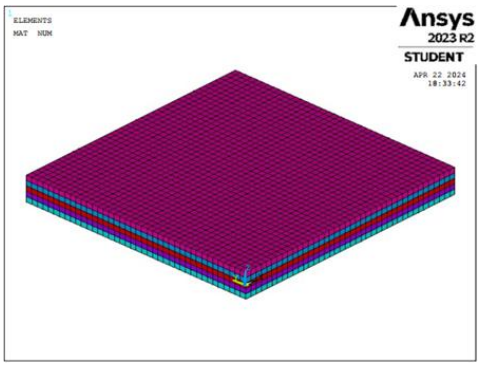

Figure 5. FG-CNTRC plate model under the effect of uniaxial load in ANSYS simulation

Table 1: Various input model scenarios.

Type	η_1	η_2	η_3	Vcnt*
1	1.2833	1.0556	1.0556	0.12
2	1.3414	1.7101	1.7101	0.17
3	1.3238	11.7380	1.7380	0.28

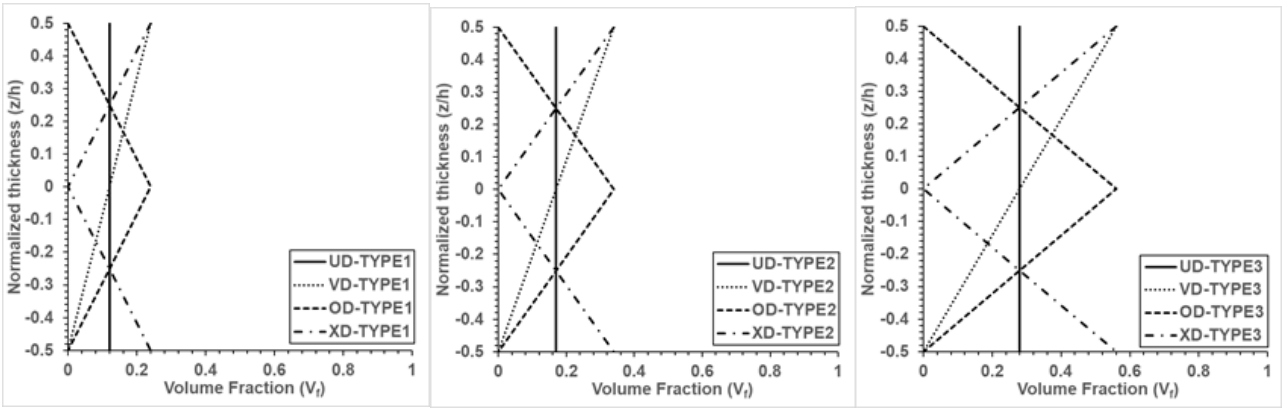

Figure 7. Illustration of volume fraction change of FG-CNT across thickness.

4.1. Results of Buckling Analysis

Table 2 and 3 displays the uniaxial buckling load factors of plates for various configurations of the FG-CNT and micromechanical model. It was demonstrated that the values acquired in this investigation were compatible with FEM (Ansys). From largest to smallest, the non-dimensional buckling load values of FG-CNTRC plate are XD>UD>VD>OD (Fig. 8). Table 2 and Table 3 show buckling load values of thick and thin plates at various material configurations for (0°/0°/0°/0°/0°) and (0°/90°/0°/90°/0°) angle orientations. In the case of the thick plate and FG-OD configuration, the dimensionless buckling load values obtained for the angle orientation (0°/0°/0°/0°/0°) are bigger than the obtained dimensionless buckling load values for the angle orientation (0°/90°/0°/90°/0°). In the case of FG-VD, the dimensionless buckling load values is nearly equal for (0°/0°/0°/0°/0°) and (0°/90°/0°/90°/0°) angle orientation. In the cases of FG-UD and FG-XD configurations, the dimensionless buckling load values obtained for the angle orientation (0°/0°/0°/0°/0°) are smaller than the obtained dimensionless buckling load values for the angle orientation (0°/90°/0°/90°/0°) (Table 2). In the case of the thin plate and FG-OD configuration, the dimensionless buckling load values obtained for the angle orientation.

(0°/0°/0°/0°/0°) are bigger than the obtained dimensionless buckling load values for the angle orientation (0°/90°/0°/90°/0°). In the case of FG-VD, the dimensionless buckling load values obtained for the angle orientation (0°/0°/0°/0°/0°) are bigger than the obtained dimensionless buckling load values for the angle orientation (0°/90°/0°/90°/0°). In the cases of FG-UD and FG-XD configurations, the dimensionless buckling load values obtained for the angle orientation (0°/0°/0°/0°/0°) are smaller than the obtained dimensionless buckling load values for the angle orientation (0°/90°/0°/90°/0°) (Table 3). Furthermore, it is observed that the order of buckling loads of plate in terms of Vf and η parameters for micromechanical models is Type3>Type2>Type1 (Fig. 8 and 9).

Table 2: Uniaxial dimensionless buckling load values of thick plate for various micromechanical models and angle orientations. (b/h= 10)

Lamina Type	FGCNT Type	FG-OD		FG-VD		FG-UD		FG-XD	
		This study (calculated)	This study (Ansys)	This study (calculated)	This study (Ansys)	This study (calculated)	This study (Ansys)	This study (calculated)	This study (Ansys)
0°/0°/0°/0°/0°	1	10.2924	9.9439	16.9101	16.4612	23.9966	24.1484	32.9210	32.8386
	2	15.8196	15.4540	26.2284	25.7405	37.5424	37.8325	52.9845	52.2735
	3	21.2110	20.6679	37.1433	36.0871	52.1664	52.4314	75.6030	70.3509
0°/90°/0°/90°/0°	1	9.04446	8.82948	17.1570	17.6612	26.4296	27.3353	36.3845	37.1730
	2	13.1716	12.9755	26.3042	27.5104	40.8121	42.4951	57.7196	58.7546
	3	16.2769	15.9007	37.0253	37.3599	58.5435	60.1049	84.0559	81.0153

Table 3: Uniaxial dimensionless buckling load values of thin plate for various micromechanical models and angle orientations. (b/h= 40)

Lamina Type	FGCNT Type	FG-OD		FG-VD		FG-UD		FG-XD	
		This study (calculated)	This study (Ansys)	This study (calculated)	This study (Ansys)	This study (calculated)	This study (Ansys)	This study (calculated)	This study (Ansys)
0°/0°/0°/0°/0°	1	11.4556	11.5168	21.1054	20.8858	34.2187	34.4356	56.2738	56.5251
	2	17.3478	17.4885	31.8347	31.4398	51.3572	51.7556	84.896	85.2889
	3	23.8512	23.9606	47.0617	46.7938	78.8232	79.2238	133.563	132.988
0°/90°/0°/90°/0°	1	10.315	10.4501	19.7247	21.3463	34.4983	35.8408	56.7926	58.4774
	2	14.6815	15.0779	29.7241	32.4741	51.7094	54.0506	85.5411	88.4675
	3	18.3072	18.6433	42.7954	45.5032	79.6236	82.1985	134.898	137.791

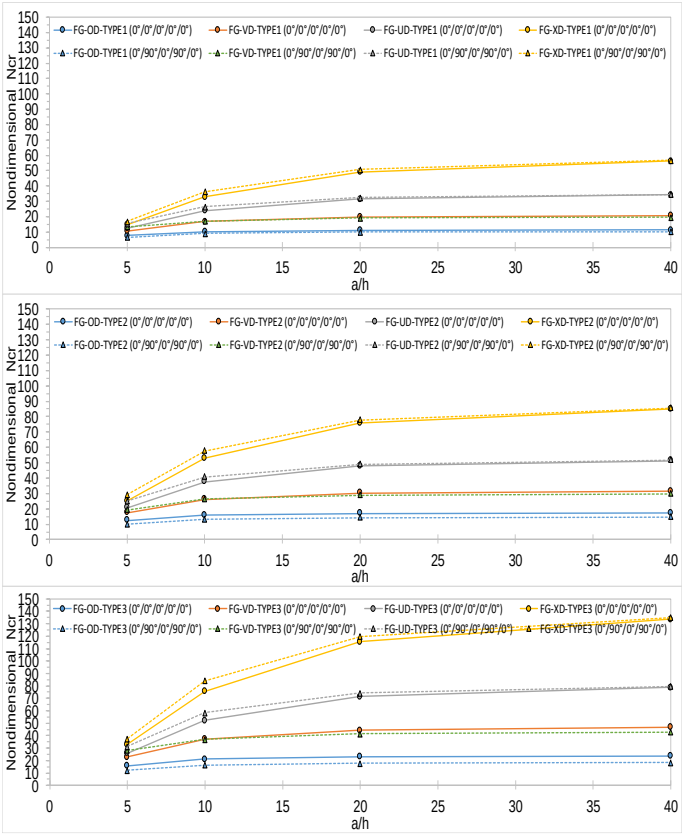

Figure 8. Effect of thickness ratio on non-dimensional Ncr values for varied configurations of the FG-CNT

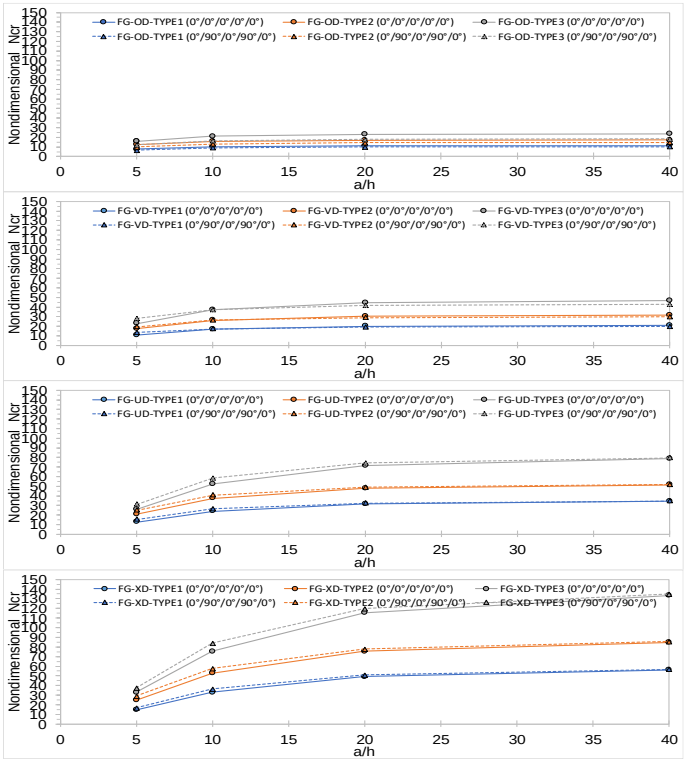

Figure 9. Effect of thickness ratio on non-dimensional Ncr values for various FG-CNT micro-mechanical models

4.2. Results of Free Vibration Analysis

Table 4 and 5 displays the non-dimensional free vibration of rectangular plates for various configurations of the FG-CNT and micromechanical model. It was demonstrated that the values acquired in this investigation were compatible with FEM (Ansys). From largest to smallest, the non-dimensional free vibration values of FG-CNTRC plate are XD>UD>VD>OD (Fig. 10). Table 4 and Table 5 show non-dimensional frequency values of thick and thin plates at various material configurations for (0°/0°/0°/0°/0°) and (0°/90°/0°/90°/0°) angle orientations. In the case of thick plate, FG-OD configuration, the dimensionless free vibration values obtained for the angle orientation (0°/0°/0°/0°/0°) and (0°/90°/0°/90°/0°) is nearly equal. In the case of FG-VD configuration, the dimensionless free vibration values obtained for the angle orientation (0°/0°/0°/0°/0°) and (0°/90°/0°/90°/0°) are very closed to each other. In the cases of thick plate, for FG-UD and FG-XD configurations, the dimensionless buckling load values obtained for the angle orientation (0°/0°/0°/0°/0°) are smaller than the obtained dimensionless free vibration values for the angle orientation (0°/90°/0°/90°/0°) (Table 4). In the cases of the thin plate, for FG-UD and FG-XD configurations, the dimensionless free vibration values obtained for the angle orientation (0°/0°/0°/0°/0°) and (0°/90°/0°/90°/0°) is nearly equal (Table 5). In the cases of FG-VD configurations, the dimensionless free vibration values obtained for the angle orientation (0°/0°/0°/0°/0°) are bigger than the obtained dimensionless free vibration values for the angle orientation (0°/90°/0°/90°/0°). In the cases of FG-OD configuration, the dimensionless free vibration values obtained for the angle orientation (0°/0°/0°/0°/0°) and (0°/90°/0°/90°/0°) is nearly equal (Table 5). Furthermore, in terms of Vf and η parameters for micromechanical models, it is observed that the order of dimensionless free vibration results of FG plate is Type3>Type2>Type1 (Fig. 10 and 11).

Table 4: Uniaxial non-dimensional frequency values of thick plate for various micromechanical models and angle orientations. (b/h= 10)

Lamina Type	FGCNT Type	FG-OD		FG-VD		FG-UD		FG-XD	
		This study (calculated)	This study (Ansys)	This study (calculated)	This study (Ansys)	This study (calculated)	This study (Ansys)	This study (calculated)	This study (Ansys)
0°/0°/0°/0°/0°	1	9.92642	9.71884	12.43928	12.68808	15.14387	15.14387	17.71050	17.64189
	2	12.26296	12.06023	15.73105	15.47320	18.85736	18.85736	22.34867	22.12538
	3	14.09624	13.86914	18.55677	18.21420	22.03037	23.03037	26.40694	25.41685
0°/90°/0°/90°/0°	1	9.96028	9.765542	12.76998	12.44063	15.89906	15.86907	18.62800	18.56395
	2	12.27211	12.07946	15.73974	15.38373	19.66736	19.63568	23.33519	23.15083
	3	14.13281	13.91246	18.50565	17.99844	23.34959	23.35682	27.85931	27.00512

Table 5: Uniaxial non-dimensional frequency values of thin plate for various micromechanical models and angle orientations. (b/h= 40)

Lamina Type	FGCNT Type	FG-OD		FG-VD		FG-UD		FG-XD	
		This study (calculated)	This study (Ansys)	This study (calculated)	This study (Ansys)	This study (calculated)	This study (Ansys)	This study (calculated)	This study (Ansys)
0°/0°/0°/0°/0°	1	10.53883	10.52234	14.19875	14.17551	18.17673	18.17673	23.26160	23.25151
	2	12.92424	12.90862	17.34592	17.32301	22.17253	22.17255	28.42477	28.39466
	3	15.04084	15.02268	20.96553	20.93270	27.21381	27.21379	35.25883	35.09753
0°/90°/0°/90°/0°	1	10.54133	10.52615	13.79763	13.77024	18.25083	18.25078	23.36860	23.36798
	2	12.92491	12.91027	16.86497	16.83622	22.24842	22.24808	28.53257	28.51735
	3	15.04356	15.02624	20.04805	20.00564	27.35217	27.35165	35.43470	35.32911

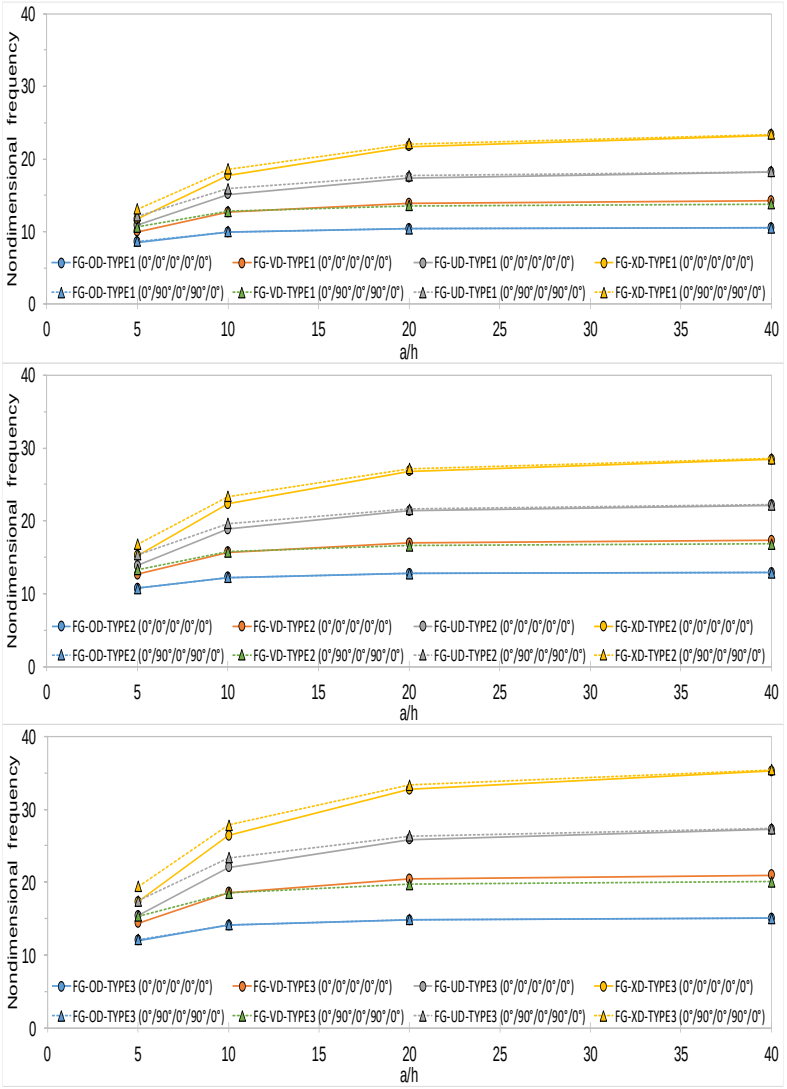

Figure 10. Effect of thickness ratio on non-dimensional frequency values for varied configurations of the FG-CNT

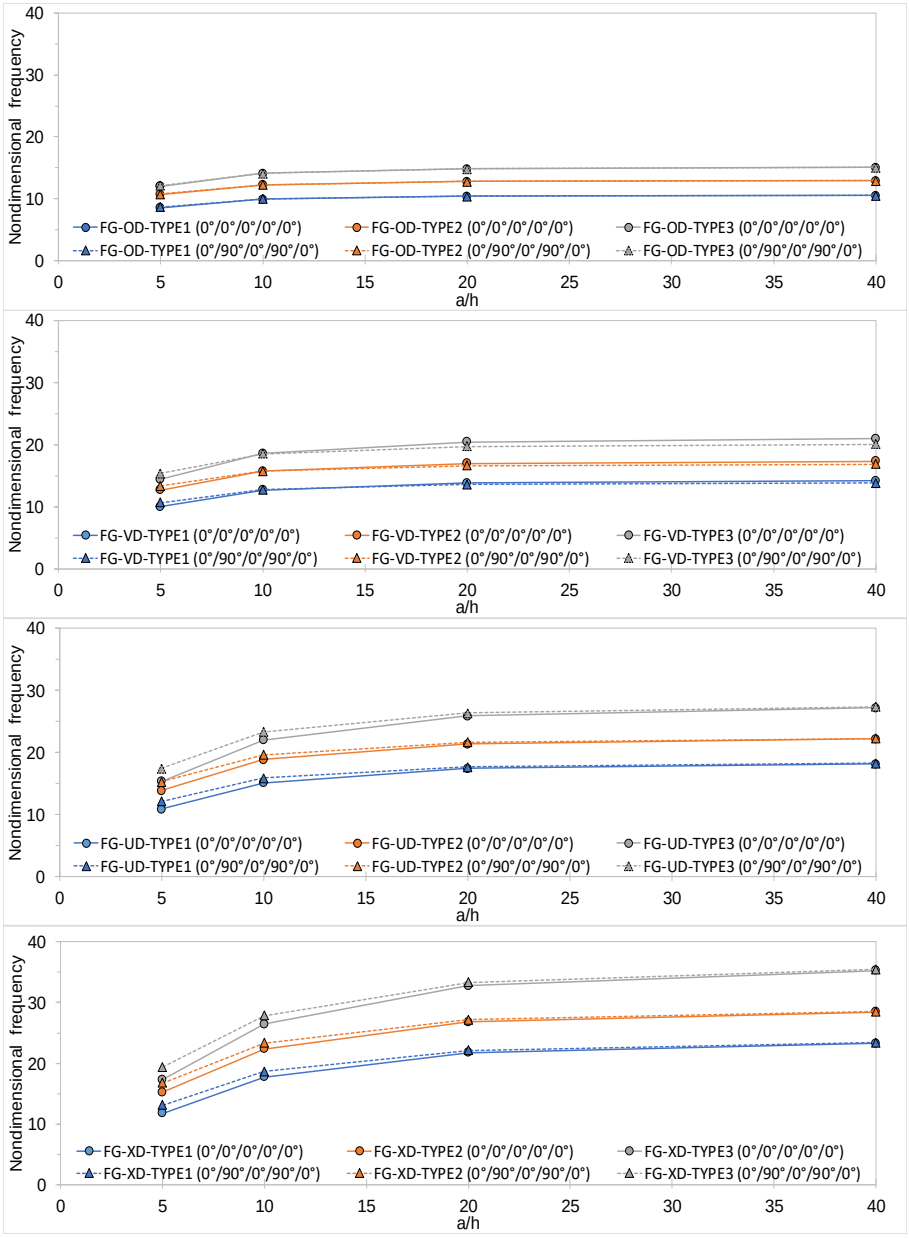

Figure 11. Effect of thickness ratio on non-dimensional frequency values for various FG-CNT micro-mechanical models

5. Conclusions

The present study investigated the buckling and free vibration analysis of rectangular plates reinforced with FG-CNTRC material under uniaxial loads. The FG-CNTRC material was put into the plate both layered and at an angle within each lamina. The governing equation for the FGCNT material-reinforced plate was obtained by applying Hamilton's principle. The solutions were done by using Navier solution method. The critical buckling load values were computed in this work for FG-OD, FG-VD, FG-UD and FG-XD distributions of CNT over the thickness of plate. The results of the research were compared with the results obtained with the help of ANSYS. The approach employed in this study is totally congruent with the results obtained using the ANSYS. Then, a parametric study was performed to better comprehend the effect of a/h ratios and V_f for various micromechanical models and FG-CNT combinations. The results obtained are summarized as follows:

- The non-dimensional buckling loads and free vibration frequency parameters obtained for calculated with this study were detected to be compatible with FEM (Ansys) results.
- The effect of thickness ratios (a/h), volume ratios (V_{cnt}^*) and efficiency parameters (η) for several micromechanical models and FG-CNT configurations have a very significant effect on buckling loads and free vibration frequency parameters.
- The increase rate of dimensionless buckling load factors increases from Type1 to Type3. In other

words, when the a/h ratio increases, the dimensionless buckling load factor curves in Type 1 are more horizontal. They are not affected much by the increase in the a/h ratio. However, when the a/h values increase in Type 3, the dimensionless buckling load values increase significantly.

- The smallest dimensionless buckling load values occur in the case of FG-OD configurations and the largest dimensionless buckling load values occur in the case of FG-XD configurations.
- When the plate thickness decreases, that is, as the a/h ratio increases, buckling loads and frequency values both increase and the rate of increase increases.
- As the plate thickness decreases, that is, as the a/h ratio increases, the rate of increase in buckling loads and frequency values occurs the most in FG-XD. The order of increase rate is FG-XD> FG-UD> FG-VD> FG-OD.
- Micromechanical models appear to importantly affect buckling loads and and free vibration frequency parameters. A suitable change in FG configurations, and volume fractions can enable the manufacture of smart products that intelligently respond to engineering problems and suit the needs.
- Knowing the behavior of plates and shells containing FG-CNT under the influence of axial load is important in sectors where many high-tech products are used (aerospace engineering, rocket technology, automotive and engine technology, civil engineering, etc.). By optimizing the FG-CNT material configurations and volume fractions required for these technologies, smart materials tailored to the required function can be composed.
- In future work, stress and strain distributions along the length of laminate sheets and failure theories can be examined. FG-CNT laminated plate types can be examined using optimization techniques.

Article Information

Financial Disclosure: The author (s) has no received any financial support for the research, authorship or publication of this study.

Authors' Contrtibution: Concept: Doğan; Design: Doğan; Supervision: Doğan; Resources: Doğan; Data Collection: Doğan; Analysis: Doğan; Literature Search: Doğan; Writing Manuscript: Doğan; Critical Review: Doğan.

Conflict of Interest/Common Interest: Not applicable.

Ethics Committee Approval: Not applicable**.**

Declaration of the Author(s): The author(s) declare that there is no conflict of interest regarding the publishing of the paper by the Journal of Innovative Science and Engineering, that the paper has been not published elsewhere, and not include any form of plagiarism. All the authors listed above have approved the manuscript and have agreed with the submission of the manuscript to the Journal of Innovative Science and Engineering.

References

[1] Yas, M. H., and Samadi, N. (2012). Free vibrations and buckling analysis of carbon nanotube-reinforced composite Timoshenko beams on elastic foundation, *International Journal of Pressure Vessels and Piping*, 98: 119-128.

[2] Lei, Z. X., Zhangc, L.W., and Liew, K., M. (2015). Buckling of FG-CNT reinforced composite thick skew plates resting on Pasternak foundations based on an element-free approach. *International Journal of Pressure Vessels and Piping*, 266: 773-791.

[3] Kumar, P., and Srinivas, J. (2017). Free vibration, bending and buckling of a FG-CNT reinforced composite beam, Comparative analysis with hybrid laminated composite beam. *Multidiscipline Modeling in Materials and Structures*, 13(4): 590-611.

[4] Civalek, Ö., Dastjerdi, S., and Akgöz, B. (2020). Buckling and free vibrations of CNT-reinforced cross-ply laminated composite plates", *Mechanics Based Design of Structures and Machines*, 98:119-128.

[5] Dastjerdi, R. M., and Mohammadi, H. M. (2017). Free Vibration and Buckling Analyses of Functionally Graded Nanocomposite Plates Reinforced by Carbon Nanotube", *Mechanics of Advanced Composite Structures*, 4**:** 59-73.

[6] Nguyen, P. D., Papazafeiropoulos, G., Vu Q. V., and Duc N. D. (2022). Buckling response of laminated FG-CNT reinforced composite plates: Analytical and finite element approach. *Aerospace Science and Technology*, 121: 107368.

[7] Foroutan, K., Carrera, H., and Ahmadi, H. (2021). Static and dynamic hygrothermal post buckling analysis of sandwich cylindrical panels with an FG-CNTRC core surrounded by

nonlinear viscoelastic foundations. *Composites Structures,* 259: 113214.

[8] Efraim, E., and Eisenberger, M., (2007). Exact vibration analysis of variable thickness thick annular isotropic and FGM plates. Journal of Sound and Vibration, 299: 720-738. doi:10.1016/j.jsv.2006.06.068

[9] Nguyen, T. K., Karam Sab, K., and Bonnet, G. (2008). First-order shear deformation plate models for functionally graded materials. Composite Structures, 83: 25-36. doi:10.1016/j.compstruct.2007.03.004

[10] Zhang, L. W., Lei, Z. X., and Liew, K. M. (2015). Buckling analysis of FG-CNT reinforced composite thick skew plates using an element-free approach. Composites Part B, 75: 36-46.

[11] Kiani, Y. (2016). Free vibration of functionally graded carbon nanotube reinforced composite plates integrated with piezoelectric layers. Computers and Mathematics with Applications, 72: 2433-2449. doi.org/10.1016/j.camwa.2016.09.007

[12] Kiani, Y. (2016). Shear buckling of FG-CNT reinforced composite plates using Chebyshev-Ritz method. Composites Part B, 105: 176-187. doi.org/10.1016/j.compositesb.2016.09.001

[13] Kiani, Y. (2017). Buckling of FG-CNT-reinforced composite plates subjected to parabolic loading. Acta Mechanica, 228: 1303-1319. DOI 10.1007/s00707-016-1781-4

[14] Mota, A. F., Loja, M. A. R., Barbosa, J. I., and Rodrigues, J. A. (2020). Porous Functionally Graded Plates: An Assessment of the Influence of Shear Correction Factor on Static Behavior. Mathematical and Computational Applications, 25 (2): 1-25. doi:10.3390/mca25020025

[15] Sahan, M. F. (2015). Transient analysis of cross ply laminated shells using FSDT: Alternative formulation. Steel and Composite Structures, 18(4), 889-907., Doi: 10.12989/scs.2015.18.4.889

[16] Sahan, M. F. (2016). Dynamic analysis of linear viscoelastic cross-ply laminated shallow spherical shells. Composite Structures,149: 261-270. Doi: 10.1016/j.compstruct.2016.04.045

[17] Dogan, A. (2009) Free Vibration analysis of laminated composites plates and cylindrical shallow shells. Ph.D. Thesis, Çukurova University, Adana, Türkiye.

[18] Dogan, A. (2012). Investigation of the effect of shell plan-form dimensions on mode-shapes of the laminated composite cylindrical shallow shells using SDSST and FEM. *Steel and Composite Structures*, 12 (4): 303-324.

[19] Dogan, A. (2018). The effect of curvature on transient analysis of laminated composite cylindrical shells on elastic foundation". *Pamukkale University Journal of Engineering Sciences (PAJES)*, 24(6): 960-966.

[20] Dogan, A. (2019). Buckling Analysis of Symmetric Laminated Composite Plates.: ISTE-CE'xx2019- International Conference on Innovation, Sustainability, Technology and Education in Civil Engineering, 13-15 June, 2019, Iskenderun, Hatay / TURKIYE., 2019.

[21] Dogan, A. (2020). Buckling analysis of laminated composite plates under the effect of uniaxial and biaxial loads. *Turkish Journal of Engineering (TUJE),* 4(4): 218-225.

[22] Dogan, A. (2022). Quasi-static and dynamic response of functionally graded viscoelastic plates. *Composite Structures*, 280, 114883.

[23] Dogan, A and Sahan, M. F. (2023) Viscoelastic damped response of laminated composite shells subjected to various dynamic loads. Mechanics Based Design of Structures and Machines, 51(8):4685-4708. doi.org/10.1080/15397734.2021.1975296

[24] Dogan, A. (2024). Dynamic response of laminated functionally graded carbon nanotube-reinforced composite viscoelastic plates. *Mechanics Based Design of Structures and Machines, 52(8):5562-5589.*

[25] Dogan, A. (2025). Dynamic and quasi-static behavior of laminated FG-CNTRC viscoelastic double-curved shells. Mechanics Based Design of Structures and Machines. doi.org/10.1080/15397734.2025.2466645

[26] Temel, B., and Sahan, M. F. (2013). An alternative solution method for the damped response of laminated Mindlin plates. Composites: Part B, 47: 107-117.doi.org/10.1016/j.compositesb.2012.10.039

[27] Özbey, M. B., and Calim, F. F. (2025). Dynamic analysis of viscoelastic functionally graded nanoplate. Mechanics Based Design of Structures and Machines. doi.org/10.1080/15397734.2024.2449481

[28] Yildirim, S., and Tutuncu, N. (2024). Inertio-elastic instability of functionally graded nanotube-reinforced composite disks. The Journal of Strain Analysis for Engineering Design, 75: 36-46. doi.org/10.1177/03093247241302911

[29] Noori, A. R., and Temel, B. (2021). A powerful numerical approach for the axisymmetric bending response of shear deformable two-directional functionally graded (2D-FG) plates with variable thickness. Proceedings of the Institution of Mechanical Engineers, Part C: Journal of Mechanical Engineering Science, 235(22): 6370-6387. doi.org/10.1177/09544062211010837

[30] Temel, B., and Sahan, M. F. (2013). Transient analysis of orthotropic, viscoelastic thick plates in the Laplace domain. European Journal of Mechanics - A/Solids, 37: 96-105. doi.org/10.1016/j.euromechsol.2012.05.008.

[31] Rasoli, H., Noori, A.R., and Temel B. (2024). Static analysis of functionally graded porous beam-column frames by the complementary functions method. Structures, 62: 106136. doi.org/10.1016/j.istruc.2024.106136

[32] Xiao, J., Li, S., Li, M., Fu, Y., Yan, L., Song, X., and Ke, Y. (2020). Electric field-assisted alignment of carbon nanotubes in the interlayers of CFRP composites to enhance the properties, 190: 108706. doi.org/10.1016/j.compositesa.2024.108706

[33] Cao, S., Yan, X., Zhang, Y., Wu, X., Wang, L., Shi, B., Li, K., Feng, C, Wang, Q., and Wu, B. (2025). Mechanical Performance of Diamine Silane Modified Carbon Nanotubes Reinforced Epoxy Resin Composites. Coatings, 15(1):60. doi.org/10.3390/coatings15010060

[34] Wolfram Research, Inc. (2017). Mathematica (Version 11.1) [Computer software]. http://www.wolfram.com/

[35] Swanson Analysis System Inc. (2023). ANSYS (Release 23) [Computer software]. http://www.ansys.com/